Adaptive Autocorrelation Based Heart Rate Estimation from Single-Axis Seismocardiogram: A Comprehensive Benchmark Across Six Diverse Datasets

Ajdar Ullah[1], Ismail Elnaggar[1], Sepehr Seifizarei[1], Olli Lahdenoja[1], Usman Azmat[1], Jussi Jaakkola[2], Samuli Jaakkola[2], Tuija Vasankari[2], Juhani Airaksinen[2], Tuomas Kiviniemi[2], Tero Koivisto[1], and Pasi Liljeberg[1]

***Abstract*— We introduce AACFD (Adaptive Autocorrelation Function Detector), a lightweight, fully automatic pipeline for estimating window-averaged heart rate (HR) from a single-axis seismocardiogram (SCG) without ECG calibration or machine learning. AACFD combines two periodicity detectors—(i) a YIN-style difference-function analysis of an adaptive SCG envelope and (ii) a short-window autocorrelation branch—operating on 3 s segments. The two branches are fused by feature-aware weighting based on signal-quality indices and multi-scale features; and a Hampel filter plus temporal consistency checks remove outlier windows. The algorithm is efficient enough for real-time implementation on commodity hardware.**

AACFD was validated on 535 subjects spanning six heterogeneous datasets (sampling rates 200 Hz–5 kHz): laboratory mechanocardiograms (MCG), controlled-breathing SCG (CEBS), motion-rich multichannel SCG (MC-SCG), valvular heart-disease clinics (VHD), invasive right-heart catheterization (RHC), and smartphone recordings from 300 atrial-fibrillation/sinus-rhythm subjects. For each recording we analyzed non-overlapping windows of 10, 20, 30, and 60 s and compared the SCG-derived mean HR with ECG-derived (or telemetry) reference values. After ECG- and SCG-based quality control and temporal refinement, the mean *per-subject* mean absolute error (MAE) on 30-s windows was 0.99 bpm in MCG, 0.72 bpm in CEBS, 4.38 bpm in VHD, 1.34 bpm in MC-SCG after removal of recordings with corrupted ECG, 3.58 bpm in RHC, and 7.67 bpm in the smartphone cohort. Across all datasets, more than 90% of non-overlapping 10–60 s windows passed ECG- and SCG-based quality control, so the reported errors reflect nearly the full usable recording duration rather than a few selected clean segments.

This cross-dataset benchmark indicates that a short-window hybrid YIN and autocorrelation routine, guarded by simple robustness checks, attains sub-bpm accuracy on resting datasets and clinically acceptable accuracy on several pathological cohorts using only a single accelerometer axis. Importantly, AACFD is deliberately designed and evaluated for reliable *window-averaged* HR estimation on 10–60 s time scales rather than instantaneous beat-to-beat HR; deriving robust heart-rate-variability indices from SCG remains an important direction for future work.

***Index Terms*— Autocorrelation, Heart Rate Estimation, Seismocardiography, Mechanocardiography, Signal Processing, Wearable Devices.**

I. Introduction

HEART rate (HR) monitoring is a foundation of cardiovascular research and clinical diagnostics, and its accurate estimation remains critical for both clinical and consumer applications. In recent years, wearable devices have gained prominence due to their ability to continuously capture physiological signals using embedded inertial and optical sensors. Among these modalities, ballistocardiography (BCG) and seismocardiography (SCG) have emerged as non-invasive methods for estimating HR by measuring the mechanical vibrations produced by the heart [1], [2].

BCG captures the complete body recoil of blood ejection, usually through sensors in beds or chairs, while SCG measures local chest vibrations directly related to cardiac mechanical events by placing an inertial sensor or smartphone on the sternum, offering a non-invasive window into cardiovascular function for wearable long-term unobtrusive monitoring [3]–[5]. This capability is particularly valuable in settings where traditional electrocardiography (ECG) may be impractical, such as home-based health monitoring or cardiac disease screening outside of clinical environments [6]. Nevertheless, extracting a reliable HR from SCG signals presents considerable challenges. The principal difficulty stems from the susceptibility of SCG signals to motion artifacts, respiratory movements, and ambient noise, all of which can corrupt or obscure the subtle cardiac-induced vibrations [7]. In parallel with ECG, BCG, and SCG, photoplethysmography (PPG) is used by many consumer wearables for pulse-rate monitoring.

Research supported by INSIDE-HEART project (INSIDE-HEART, 2023), which has received funding from the European Union's Horizon Europe program under the Marie Skłodowska Curie grant agreement No 101119941.

[1]A. Ullah, I. Elnaggar, S. Seifizarei, O. Lahdenoja, U. Azmat, T. Koivisto, and P. Liljeberg are with the Department of Computing, University of Turku, Turku 20014, Finland (email: ajulla@utu.fi; ismail.m.elnaggar@utu.fi; sepehr.seifizarei@utu.fi; olanla@utu.fi; usman.azmat@utu.fi; tejuko@utu.fi; pasi.liljeberg@utu.fi).

[2]J. Jaakkola, S. Jaakkola, T. Vasankari, T. Kiviniemi and J. Airaksinen are with the Heart Center, Turku University Hospital and University of Turku, 20014, Finland (email: jussi.jaakkola@utu.fi; skjaak@utu.fi; tuija.vasankari@varha.fi; Juhani.Airaksinen@tyks.fi; Tuomas.Kiviniemi@tyks.fi).

Wrist-worn and fingertip PPG sensors are inexpensive and convenient, but optical measurements are sensitive to motion artifacts, vasomotor tone, and perfusion changes, particularly in cold environments or during exercise [8]. SCG and related cardio-mechanical modalities are attractive complements because they measure mechanical activity closer to the heart and can be implemented using the same inertial sensors already present in smartphones and many wearables. Most recent SCG studies therefore target *instantaneous* HR and HR variability (HRV), i.e., beat-to-beat intervals, often using sophisticated peak-detection, probabilistic, or learning-based schemes [9]–[16]. By contrast, the present work focuses on a simpler but practically relevant question: how can we obtain accurate *mean* HR on short windows (10–60 s) from a single SCG axis without ECG calibration or machine learning, across heterogeneous cohorts and recording setups? We deliberately do not attempt beat-to-beat HR or HRV estimation here; those remain important directions for future work.

Focusing on window-averaged HR is nonetheless practically relevant. Many wearable and home-monitoring applications require a robust mean HR every 10–60 s, rather than full HRV, and must operate under tight power, memory, and regulatory constraints where heavy machine-learning models are undesirable. Our goal is therefore not to outperform state-of-the-art beat-level detectors, but to show that a lightweight, interpretable SCG-only pipeline can provide clinically acceptable mean HR across heterogeneous datasets without ECG calibration.

We put our method to the test across six diverse datasets, encompassing a range of recording setups and sensor types. Five of these are publicly available, totaling 235 subjects: Mechanocardiograms with ECG reference (MCG dataset) (N=29) [17], Combined measurement of ECG, Breathing and Seismocardiograms dataset (CEBS dataset) (N=20) [18], SCG-RHC: Wearable Seismocardiogram Signal and Right Heart Catheter Database (SCG-RHC dataset) (N=73) [19], An Open-access Database for the Evaluation of Cardio-Mechanical Signals from the patients with Valvular Heart Diseases dataset (VHD dataset) (N=100) [20], and Multichannel Seismocardiography dataset (MC-SCG dataset) (N=13) [21]. The sixth is a closed dataset, previously reported by Iftikhar and Jaakkola *et al.*, which includes data from 300 subjects [22], [23]. While the total subject count for the open-access datasets is 235, the closed dataset adds further validation under distinct conditions, such as mobile device-based recordings. This broad evaluation highlights the method's adaptability across varied contexts.

The objectives of this study are (1) to develop a reliable mean-HR estimation framework for SCG without the need for concurrent ECG, except as a reference gold standard, and (2) to evaluate its performance in a broad set of datasets to provide a practical benchmark for the community. Our approach combines established techniques—multi-stage filtering and autocorrelation—with refinements such as iterative thresholding and outlier correction, and applies them consistently across six heterogeneous SCG/MCG cohorts, including both open and closed datasets. This work advances the field by offering a versatile tool for non-invasive cardiovascular monitoring, with applications in wearable health technologies.

Several earlier studies from our group have also used autocorrelation on cardio-mechanical signals. Iftikhar *et al.* [22] applied short-term autocorrelation of smartphone mechanocardiograms only as hand-crafted *features* for a multiclass AF/SR classifier, without estimating HR from the autocorrelation curve or reporting SCG–ECG HR errors. More recently, Ullah *et al.* proposed a preliminary autocorrelation-based HR estimator from a single-axis smartphone accelerometer, computing a single mean HR value per 3-min recording on the same closed AFib cohort [24]. That conference paper did not consider shorter analysis windows, feature-aware YIN and ACF fusion, morphology-based harmonic guards, or cross-dataset benchmarking. The AACFD algorithm presented in this paper was developed after these studies as a separate line of work: it generalises the autocorrelation idea to a hybrid YIN and ACF pipeline and systematically benchmarks window-averaged HR on 10–60 s windows across six heterogeneous SCG/MCG datasets, without reusing code from the previous work.

More recently, Elnaggar *et al.* proposed a sensor-agnostic aortic-opening peak detector based on SVMD, CWT envelopes and AMPD peaks and performed a cross-dataset validation on five open SCG corpora [25]. To our knowledge, their work was the first to report SCG-based beat-level timing and 2-s HR errors on the VHD and SCG-RHC datasets. Their focus is instantaneous HR and AO timing on very short windows. Here we evaluate AACFD (Adaptive Autocorrelation Function Detector) on the same VHD and RHC cohorts but target mean HR on longer 10–60 s windows, providing a complementary, low-complexity alternative for SCG-based HR monitoring rather than a direct competitor to beat-to-beat methods.

Contributions

The main contributions of this work are:

- We propose AACFD, a lightweight, interpretable hybrid YIN and autocorrelation pipeline for *window-averaged* HR estimation from single-axis SCG, requiring no ECG calibration or machine learning.
- We provide a unified cross-dataset benchmark of AACFD on six heterogeneous datasets (535 subjects, 584 recordings) covering healthy volunteers, VHD, AF, multichannel SCG imaging, and RHC datasets.
- We design AACFD as a hybrid YIN and autocorrelation algorithm that combines an adaptive envelope branch, feature-aware fusion, morphology-based harmonic guards, and multi-stage signal-quality and outlier handling tailored to 10–60 s windows.
- We report per-dataset MAE, RMSE, and Bland–Altman limits of agreement, across multiple window durations (10, 20, 30, 60 s), highlighting where mean-HR estimation from SCG is reliable and where pathological variability or motion still pose challenges.

II. Literature Review

A. Historical Background of SCG

SCG emerged as a distinct field in the late 20th century. Pioneering work by Salerno and Zanetti established SCG as

TABLE I
DATASETS USED FOR HR EVALUATION

Dataset	Subjects (N)	Recordings (R)	Recording Duration	Sampling rate	Key features
MCG [17]	29	29	≈5 min	800 Hz	3-axis SCG + GCG + ECG
CEBSDB [18]	20	60	60 min (5+50+5)	5 kHz	ECG, respiration, 1-axis SCG
SCG-RHC [19]	73	82	Variable (procedure length)	500 Hz / 256 Hz	Patch SCG with invasive hemodynamics
VHD [20]	100	100	≈6 min 48 s	256 Hz	Valvular heart disease patients
MC-SCG [21]	13	13	≈2 min	1 kHz	78-lead SCG array
Iftikhar (closed) [22]	300	300	3 min	200 Hz	Smartphone SCG (SR & AFib)

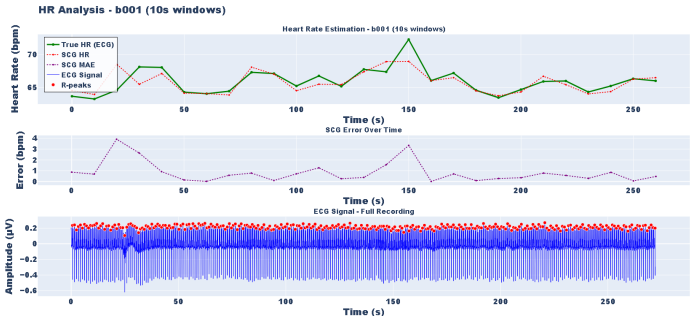

Fig. 1. Example 10 s analysis windows (subject B001 of the CEBS dataset) illustrating SCG signal, AACFD HR estimate, and window-level MAE.

a non-invasive tool for monitoring mechanical events such as heart valve closure [26], [27]. In contrast, BCG dates back to Starr's 1939 studies of whole-body recoil [28]. Recent leaps in MEMS-based inertial sensors have rekindled interest in SCG for wearable and clinical monitoring, driving its emergence as a versatile tool for non-invasive cardiovascular assessment [2], [6], [29].

B. Signal Processing Techniques for SCG

Extracting HR from SCG signals necessitates advanced signal processing to address noise from motion, respiration, and environmental sources. The following subsections outline key techniques commonly applied in the field.

1) Filtering Methods: Filtering is essential to isolate cardiac-related frequency components in SCG, typically spanning 0.5–20 Hz [30]. Butterworth filters are popular because their flat magnitude response suppresses broadband noise while preserving waveform morphology [30]–[32]. This property has made them a cornerstone of SCG signal analysis. Bessel filters, with their nearly linear phase, minimize temporal distortion and are therefore useful for locating fiducial points such as the aortic-valve opening [4], [33]. Taebi *et al.* [6] and Inan *et al.* [2] both emphasized that a sub-optimal filter can obliterate critical SCG features. Recent comparative studies recommend cascading a Butterworth high-pass with a Bessel band-pass to balance noise rejection and fidelity [33].

2) Signal Decomposition Approaches: Several authors have used time–frequency and mode-decomposition techniques to enhance SCG for HR or AO-peak detection. Choudhary *et al.* combined a modified variational mode decomposition (MVMD) front-end with a decision-rule-based post-processing scheme to extract AO–AO intervals and derive HRV indices from SCG [9]. Elnaggar *et al.* proposed a sensor-agnostic aortic-opening detector based on sparse variational mode decomposition (SVMD), continuous wavelet transform (CWT) envelopes and AMPD peaks and validated it across five SCG corpora [25]. These decomposition-based pipelines typically target beat-level timing and often achieve millisecond-level precision under controlled conditions; in contrast, AACFD focuses on robust estimation of window-averaged HR using a simpler single-axis SCG front-end.

3) Periodicity Detection with Autocorrelation: Autocorrelation is a powerful tool for uncovering periodic structure in noisy cardio-mechanical signals. By correlating a signal with a delayed version of itself, rhythmic components linked to heartbeats become visible [34]. Seifizarei *et al.* demonstrated its robustness for radar-based HR estimation under moderate noise [35]. Major challenges are choosing an appropriate lag window and suppressing spurious peaks, as noted in the differential-autocorrelation work of D'Mello *et al.* [36]. Variants such as partial autocorrelation and cepstral analysis have also been explored for beat detection [37], [38]. In our pipeline, we add an iterative threshold on the normalized autocorrelation curve to accept only high-confidence peaks, inspired by the feasibility study of Pustozerov et al. [39].

4) Outlier Removal and Signal Quality Assessment: Motion bursts and sensor artifacts can produce grossly erroneous HR estimates, so robust outlier detection is mandatory. The Hampel filter that uses a moving median and a median absolute deviation (MAD) for thresholding remains effective for biomedical time series [40], [41]. We adapt Laurino's BCG implementation [34], constraining HR to the physiological band. Complementary strategies include robust-statistics approaches and signal-quality indices derived from vibration SNR or entropy measures [42]–[44].

5) Related Work on HR Estimation from SCG: Beyond autocorrelation-based approaches, many studies have focused on instantaneous HR and HRV estimation from SCG. Choudhary *et al.* extracted HRV indices from SCG in resting subjects and showed good agreement with ECG-derived HRV [9]. Lin and Jhou jointly estimated heart and respiratory rates from resting SCG [10], and Sieciński *et al.* compared HRV indices from SCG and ECG on the CEBS database with close correspondence under controlled conditions [11]. Wahlström *et al.* used a hidden Markov model for SCG beat detection [12], Cocconcelli *et al.* proposed a high-accuracy unsupervised annotation strategy [13], and more recent works introduced probabilistic and decomposition-based peak detectors such as maximum-a-posteriori heartbeat detection from chest accelerometers [14] and high-accuracy aortic-valve-opening

Algorithm 1 AACFD: Hybrid YIN and ACF HR Estimation from Single-Axis SCG (Per Window)

Require: SCG window $x(t)$, sampling rate f_s, admissible HR range $[H_{\min}, H_{\max}]$.
Require: Optional reference ECG HR H_{ECG} for the same window.
Ensure: Window-level HR estimate $\hat{H}$ and confidence C.
Ensure: (Optional) absolute SCG–ECG error e_{abs} based on availability of reference ECG.
Notation Q_{SCG}: SCG signal-quality index (0–1). ϕ_{SQA}: SQA features; ϕ_{MS}: multiscale features. $\tilde{\phi}$: attention-weighted feature vector. H_{YIN}, H_{ACF}: HR estimates from YIN and ACF (bpm). C_{YIN}, C_{ACF}: confidences of YIN and ACF branches. P: peak-train consistency score (0–1); A: YIN–ACF agreement score.
Signal quality and feature extraction
EnhancedSQA$(x, f_s) \to (Q_{\mathrm{SCG}}, \mathrm{isNoisy}, \phi_{\mathrm{SQA}})$.
MultiScaleFeatureFusion$(x, f_s, \mathrm{isNoisy}) \to \phi_{\mathrm{MS}}$.
$\phi = \phi_{\mathrm{SQA}} \cup \phi_{\mathrm{MS}}$.
ChannelAttention$(\phi) \to \tilde{\phi}$.
Preprocessing and motion screening
AdaptivePreprocess$(x, f_s, \mathrm{isNoisy}) \to x_{\mathrm{filt}}$.
ComputeSCG_SQI_Advanced$(x_{\mathrm{filt}}, f_s) \to$ motionFlag.
if motionFlag **then**
  return ($\hat{H}$=NaN, C=0, e_{abs}=NaN).
end if
Periodicity analysis
AdaptiveEnvelope$(x_{\mathrm{filt}}, f_s, \mathrm{isNoisy}) \to e(t)$.
YIN$(e, f_s, [H_{\min}, H_{\max}]) \to (H_{\mathrm{YIN}}, C_{\mathrm{YIN}})$.
SCG_ACF$(x, f_s, [H_{\min}, H_{\max}]) \to (H_{\mathrm{ACF}}, C_{\mathrm{ACF}})$ {3-s epochs, 2-s subwindows.}
YIN–ACF fusion
FeatureAwareFusion$\big(H_{\mathrm{YIN}}, C_{\mathrm{YIN}}, H_{\mathrm{ACF}}, C_{\mathrm{ACF}}, \tilde{\phi}, Q_{\mathrm{SCG}}, \mathrm{isNoisy}\big) \to (\hat{H}_{\mathrm{fuse}}, C_{\mathrm{fuse}}, A)$.
Morphology-based harmonic guard (optional)
if $Q_{\mathrm{SCG}} > 0.4$ **and** $\phi_{\mathrm{SQA}}[\mathrm{periodicity}] > 0.3$ **then**
  Detect envelope peaks p in $e(t)$.
  ClassifyS1S2_Hybrid$(p, e, f_s, \hat{H}_{\mathrm{fuse}}) \to (S_1, S_2, \eta)$.
  Estimate H_{S_1} from RR intervals of S_1.
  if η high **and** H_{S_1} in 2:1 or 1:2 relation to $\hat{H}_{\mathrm{fuse}}$ **then**
    $\hat{H}_{\mathrm{fuse}} = H_{S_1}$.
  end if
end if
Peak-train consistency check
PeakTrainFromEnvelope$(e, f_s, \hat{H}_{\mathrm{fuse}}) \to (H_{\mathrm{env}}, P_{\mathrm{env}})$.
PeakTrainFromFiltered$(x_{\mathrm{filt}}, f_s, \hat{H}_{\mathrm{fuse}}) \to (H_{\mathrm{filt}}, P_{\mathrm{filt}})$.
$P = \max(P_{\mathrm{env}}, P_{\mathrm{filt}})$.
$C = C_{\mathrm{fuse}} \cdot (0.4 + 0.6P)$.
$\hat{H} = \hat{H}_{\mathrm{fuse}}$.
ECG comparison
if H_{ECG} is provided **then**
  $e_{\mathrm{abs}} = |\hat{H} - H_{\mathrm{ECG}}|$.
else
  $e_{\mathrm{abs}} = \mathrm{NaN}$.
end if
return $(\hat{H}, C, Q_{\mathrm{SCG}}, P, A, e_{\mathrm{abs}})$.

detection from SCG [15]. Parlato *et al.* developed a fully automated template-matching framework for ECG-free heartbeat detection in healthy and pathological cardio-mechanical signals [16]. These methods primarily target beat-level timing and HRV; in contrast, the present work focuses on robust estimation of mean HR over 10–60 s windows using a single SCG axis.

III. Datasets

We evaluated the proposed HR estimation pipeline on six publicly available or previously reported datasets. Table I lists their detailed characteristics; concise descriptions follow. **AFib dataset (closed)** (Iftikhar *et al.*) (N=300) [22]: Features mobile-device SCG recordings previously used for AF detection. **MCG dataset** (N=29) [17]: Five-minute recordings from *healthy* adults sampled at 800 Hz. Each recording provides six raw mechano-cardiac channels—a three-axis seismocardiogram from an MMA8451Q accelerometer and a three-axis gyrocardiogram from a MAX21000 gyroscope—together with a simultaneously recorded 3-lead reference ECG acquired through a Texas Instruments ADS1293 analog front-end. **CEBS dataset** (N=20) [18]: Integrates ECG, breathing, and SCG, facilitating analysis of respiratory effects. Each subject underwent a 60-min recording session comprising a 5-min basal phase, a 50-min classical-music phase, and a further 5-min rest. Signals were acquired at 5 kHz with a Biopac MP36, capturing two ECG leads, a respiratory band signal, and a single-axis SCG (z-axis). **SCG-RHC dataset** (N=73) [19]: Contains wearable SCG data collected during rest and activity, testing resilience to motion. The patch recorded SCG at 500/256 Hz, with 1 kHz ECG and simultaneous hemodynamic references from the RHC system. **VHD dataset** (N=100) [20]: Includes SCG from patients with valvular heart disease, addressing pathological variability. **MC-SCG dataset** (N=13) [21]: Offers multi-axis SCG data, supporting exploration of sensor fusion; in this work we select a single composite SCG lead (2–3–Z) to stay within the single-axis processing framework.

Collectively, the six corpora cover 235 open-source and 300 proprietary subjects, spanning healthy young volunteers, VHD patients, RHC cases, and smartphone AFib recordings, thus providing a comprehensive benchmark for single-axis SCG HR-estimation algorithms.

Table I summarizes the acquisition protocols for all six datasets. Briefly, MCG, CEBS, VHD and MC-SCG were recorded from supine or semi-supine subjects at rest in a controlled laboratory or clinical environment; CEBS additionally includes a 50-min music-listening phase with spontaneous breathing [18]. SCG-RHC was acquired from patients undergoing invasive right-heart catheterization, with chest-worn patch SCG during supine rest and procedure maneuvres [19]. The closed AFib dataset consists of 3-min smartphone SCG recordings from hospitalised AF and SR patients in semi-supine position [22]. This mix of protocols tests AACFD under both stable and procedure-related dynamic conditions.

IV. Methods

A universal hybrid periodicity detector (AACFD) was applied to all subjects. AACFD combines a refined short-window autocorrelation routine with a YIN-style envelope branch and feature-aware fusion. After preprocessing, HR estimation proceeds in three levels. (i) At the window level, each recording is split into non-overlapping windows of 10, 20, 30, or 60 s, and AACFD produces one HR estimate per window. Inside each window, the SCG is further analysed

TABLE II
FRACTION OF NON-OVERLAPPING WINDOWS RETAINED AFTER ECG- AND SCG-BASED QUALITY CONTROL.

Dataset	Window	Total	Used	Used [%]
CEBS(20/60)	10 s	7135	6707	94.0
	20 s	3571	3395	95.1
	30 s	2379	2249	94.5
	60 s	1190	1114	93.6
RHC(73/82)	10 s	11678	10757	92.11
	20 s	6041	5534	91.60
	30 s	4111	3810	92.67
	60 s	2115	1938	91.63
VHD(100/100)	10 s	4098	3884	94.8
	20 s	2053	1950	95.0
	30 s	1387	1311	94.5
	60 s	687	643	93.6
MCG(29/29)	10 s	1357	1280	94.3
	20 s	680	643	94.6
	30 s	457	426	93.2
	60 s	225	210	93.3
MC-SCG(13/13)	10 s	307	287	93.5
	20 s	153	144	94.1
	30 s	102	100	98.0
	60 s	51	46	90.2
AFib(300/300)	10 s	4800	4462	93.0
	20 s	2400	2258	94.1
	30 s	1500	1338	89.2
	60 s	600	600	100.0

in short overlapping 3-s segments. (ii) Within a window, a hybrid YIN and ACF module estimates HR from each segment and fuses these estimates based on signal-quality indices, multi-scale features, and morphology-based harmonic checks (Algorithm 1). (iii) Across windows of the same duration, temporal-consistency and outlier rules refine the HR series and suppress motion-contaminated or clearly inconsistent windows before computing error metrics. All error statistics in this paper—MAE, Bland–Altman bias, limits of agreement, and Pearson correlation (R^2) are calculated by comparing SCG-derived window HR with the mean ECG-derived HR for the same window. The complete pipeline is implemented in Python.

A. Preprocessing and Filtering

1) Signal Normalization: The raw SCG channel is centered to remove DC drift.

2) Dual Band-Pass Filtering: Butterworth and Bessel filters are applied in a sequential order. The cascade gives steep attenuation without phase distortion, isolating the quasi-periodic cardio-ballistic component while suppressing motion artifacts.

3) Sampling-Rate Harmonization: All datasets are down-sampled with anti-aliasing to $f_s = 200$ Hz for consistent processing.

B. Hybrid YIN and ACF HR Estimation (AACFD)

Algorithm 1 summarizes the hierarchical AACFD pipeline. Within each analysis window (10, 20, 30, or 60 s), the SCG $x(t)$ sampled at f_s is divided into overlapping 3-s epochs with 2-s hops; at typical resting heart rates (50–90 bpm) this yields 3–5 beats per epoch, which is sufficient for stable periodicity without excessive latency. For each epoch we first compute an SCG signal-quality index Q_{SCG} and a set of signal-quality and multi-scale features ϕ_{SQA}, ϕ_{MS} (time, frequency, non-linear, and envelope domain). A channel-attention module produces an attention-weighted feature vector $\tilde{\phi}$ that emphasises periodicity- and energy-related features and governs the subsequent preprocessing.

Preprocessing is adaptively chosen: in noisy epochs, denoising and conservative band-pass filtering are applied, whereas in cleaner epochs a lighter Butterworth–Bessel cascade is sufficient. A motion-artefact flag, derived from an advanced SCG SQI, blocks epochs dominated by gross motion. On the preprocessed SCG we derive an adaptive envelope $e(t)$ by combining a Hilbert envelope, narrow-band STFT energy, and robust squared-signal smoothing.

AACFD then uses two complementary periodicity branches on each epoch:

- **YIN branch:** a YIN-style difference function is applied to $e(t)$ over lags corresponding to 37–150 bpm. A dynamic threshold, modulated by an envelope-continuity score (regularity of inter-peak intervals and amplitudes), yields a candidate period and HR H_{YIN} with confidence C_{YIN}.
- **ACF branch:** an adaptive autocorrelation analysis is applied to the SCG, returning candidate lags and peak heights on the normalised ACF within the same HR range. Peaks must exceed an adaptive prominence threshold, resulting in an HR estimate H_{ACF} with confidence C_{ACF}.

The two estimates are fused in a feature-aware stage:

$$\hat{H}_{\mathrm{fuse}} = \frac{w_{\mathrm{YIN}} H_{\mathrm{YIN}} + w_{\mathrm{ACF}} H_{\mathrm{ACF}}}{w_{\mathrm{YIN}} + w_{\mathrm{ACF}}}, \tag{1}$$

where the weights w_{YIN} and w_{ACF} depend on C_{YIN}, C_{ACF}, Q_{SCG}, and selected features in $\tilde{\phi}$. An agreement score A penalizes large discrepancies between branches; if only one branch is valid, AACFD falls back to that branch.

For high-quality epochs ($Q_{\mathrm{SCG}} > 0.4$ and sufficiently high periodicity), a morphology-based harmonic guard is applied. Peaks in $e(t)$ are classified into S_1/S_2 using a hybrid amplitude- and timing-based Viterbi classifier, and HR is re-estimated from S_1–S_1 intervals. If this S_1 HR is in a plausible 1:2 or 2:1 relationship with $\hat{H}_{\mathrm{fuse}}$ and the classifier confidence is high, the S_1-based HR replaces $\hat{H}_{\mathrm{fuse}}$ to correct harmonic doubling or halving. Peak trains extracted independently from $e(t)$ and from the filtered SCG yield a peak-train consistency score P, which modulates the final epoch-level confidence C reported in Algorithm 1. Epochs with HR outside a broad physiological range or with very low C are discarded.

Within each 10–60-s analysis window, the remaining epoch-level HR estimates are post-processed by a Hampel filter and temporal-consistency rules (large-jump detector and validity-ratio check). If too few epochs remain, the ACF branch is optionally re-run with a more permissive threshold. The

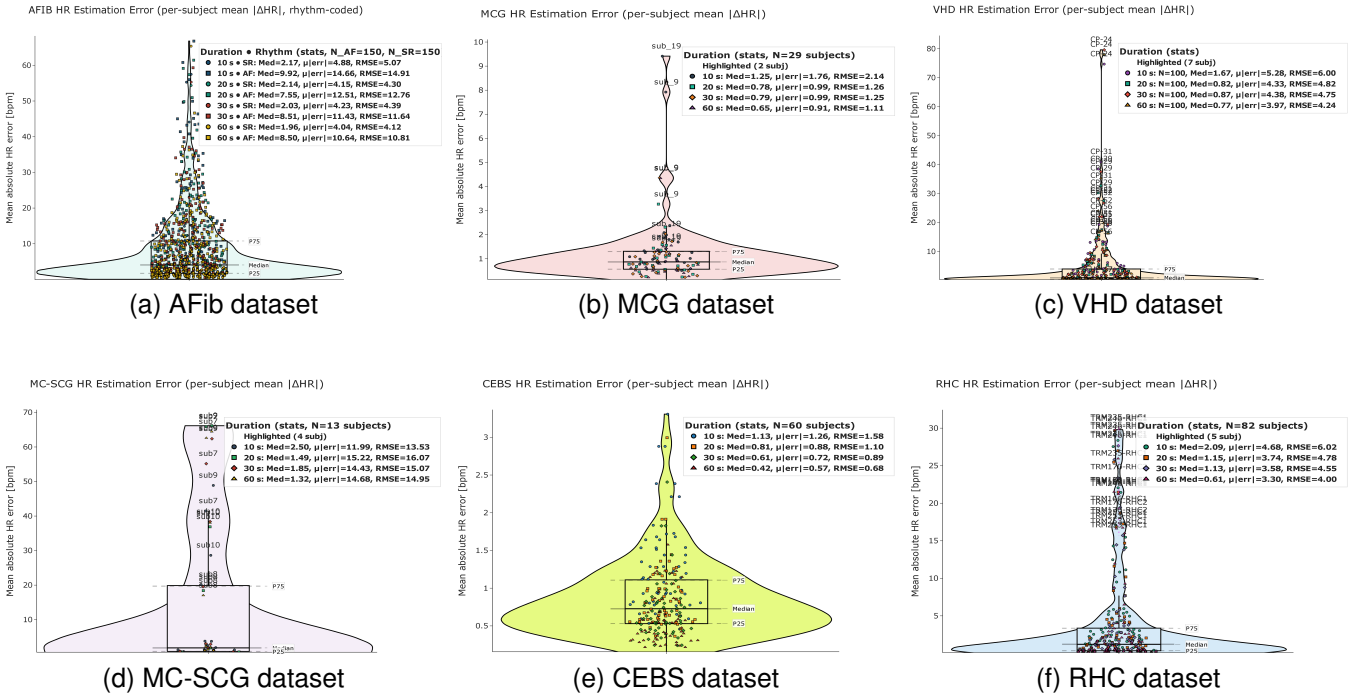

Fig. 2. Violin plots for comparison of reference ECG heart-rate with the SCG-derived estimate for six datasets: (a) AFib, (b) MCG, (c) VHD (top row), and (d) MC-SCG, (e) CEBS, (f) RHC (bottom row).

window-level HR is the average of all valid epoch HRs in that window.

Here, ϕ_{SQA} denotes the SQA feature vector (spectral kurtosis, cardiac-band energy ratio, periodicity, envelope entropy, stationarity) and ϕ_{MS} the additional multiscale time–frequency features; a light channel-attention block maps $[\phi_{\mathrm{SQA}}, \phi_{\mathrm{MS}}]$ to an attention-weighted feature vector $\tilde{\phi}$ that gates adaptive preprocessing and the feature-aware fusion of the YIN $(H_{\mathrm{YIN}}, C_{\mathrm{YIN}})$ and ACF $(H_{\mathrm{ACF}}, C_{\mathrm{ACF}})$ branches, while the peak-train consistency score P is used to modulate the final fused confidence.

C. ECG-Based True HR Measurement in Each Dataset

The ECG-based HR obtained from all open datasets was derived using NeuroKit R-peak detection [48], except for the VHD dataset, which already had annotated R-peaks. The R-peaks were visually verified and, where necessary, corrected manually. However, for the closed AFib dataset, there is no ECG signal; instead, only a single HR value was recorded during measurement.

In practice, the ECG was not always of sufficient quality across all subjects and recording locations. To avoid propagating corrupted reference signals into the HR error metrics, we therefore applied a simple ECG signal-quality assessment (ECG-SQA) in addition to the SCG-SQA described earlier. For each analysis window, we checked the plausibility and stability of the detected R-peaks (RR-interval statistics, outlier beats, and extreme rate changes) together with a local ECG noise estimate. Windows in which the ECG-SQA indicated unreliable R-peak timing or clearly non-physiological behavior were discarded and not used as reference for SCG–ECG HR error computation. The combined SCG and ECG-based SQA thus ensures that the reported MAE, RMSE, and Bland–Altman statistics are computed only from windows with both a usable SCG signal and a trustworthy ECG reference.

D. Rationale for Design Choices

A few design parameters deserve justification.

First, the 3 s analysis epochs with 2 s overlapping sub-windows in the ACF branch represent a compromise between temporal resolution and robustness. At typical resting heart rates, a 3 s segment contains 3–5 beats, which is sufficient for a stable autocorrelation pattern while still allowing tracking of rate changes. In preliminary tests on MCG and CEBS, shortening the epoch to 1 s doubled the fraction of windows with ambiguous ACF peaks, especially in pathological recordings, whereas extending it beyond 5 s increased latency without improving MAE.

Second, the lag search range of 0.4–1.6 s corresponds to 37–150 bpm and covers the vast majority of heart rates observed in all six datasets. Extending the range towards very low or very high rates increased the risk of selecting sub-harmonic or super-harmonic peaks in noisy windows, with negligible benefit in coverage.

Third, all SCG channels are down-sampled (with anti-alias filtering) to $f_s = 200$ Hz before processing. Most SCG energy relevant for beat timing lies below 30–40 Hz [30], [33], so a 200 Hz sampling rate (Nyquist 100 Hz) is sufficient to preserve morphology and timing while reducing computational load. On a subset of CEBS, down-sampling from the native 5 kHz to 200 Hz changed the 30 s-window MAE by less than 0.05 bpm on average, with no systematic bias.

This article has been accepted for publication in IEEE Journal of Biomedical and Health Informatics. This is the author's version which has not been fully edited and content may change prior to final publication. Citation information: DOI 10.1109/JBHI.2026.3665979

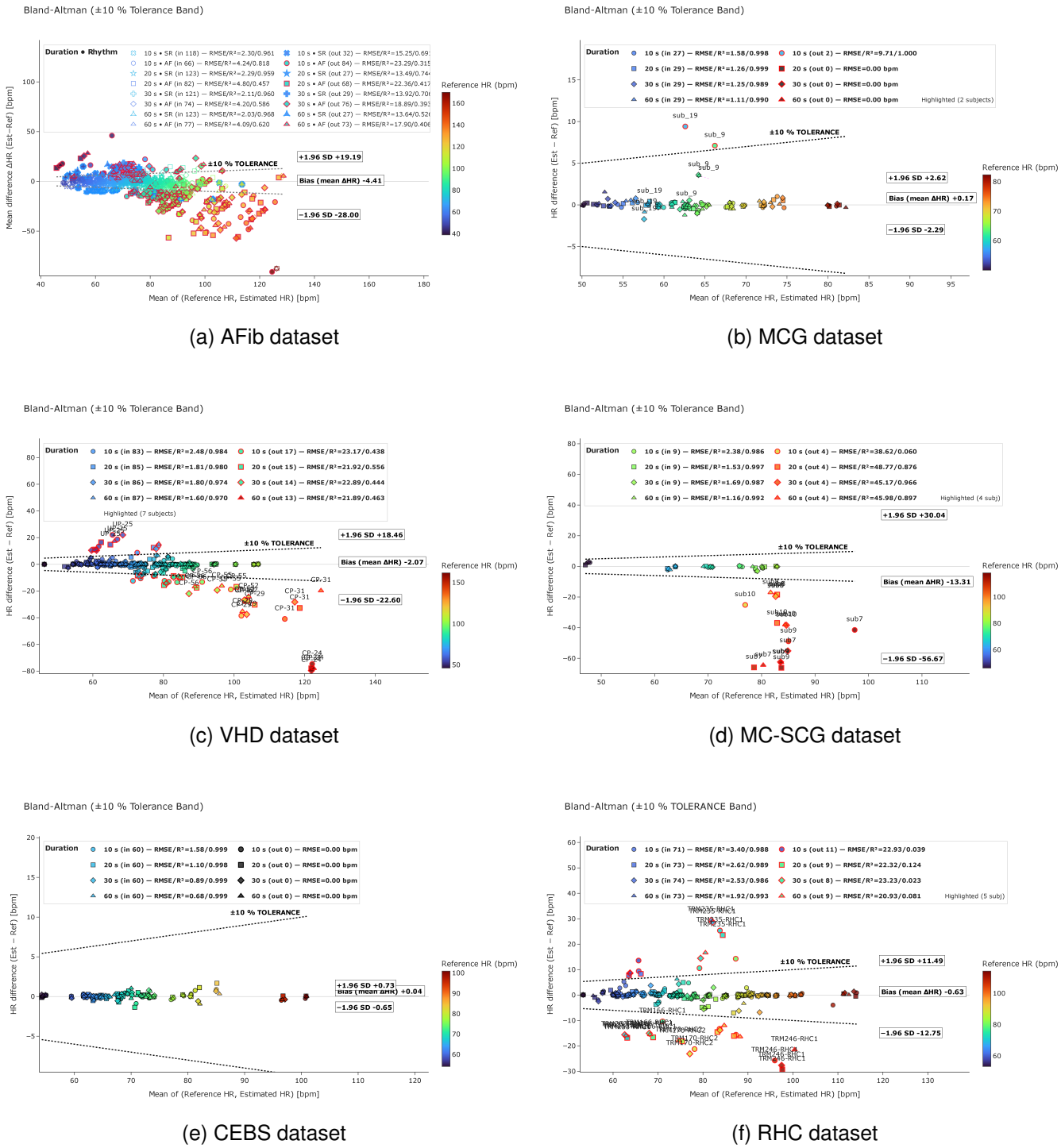

Fig. 3. Bland–Altman plots comparing reference ECG heart rate with the SCG-derived estimate for six datasets: (a) AFib, (b) MCG, (c) VHD, (d) MC-SCG, (e) CEBS, and (f) RHC.

Fig. 1 shows the HR measurement and MAE analysis for a 10 s window of subject B001 of CEBS dataset.

Fourth, the dual YIN and ACF structure and the additional robustness steps are motivated by complementary failure modes. The YIN branch is less sensitive to amplitude fluctuations and provides a robust period estimate when the envelope is clean but the raw SCG is noisy, whereas the ACF branch can still succeed when the envelope is distorted but the underlying oscillation remains coherent. The morphology-based S_1/S_2 harmonic guard is specifically designed to reduce 1:2 and 2:1 errors at high heart rates, which we observed frequently in preliminary experiments on VHD and RHC. Finally, Hampel filtering and temporal-consistency checks across epochs are essential to suppress isolated gross outliers

TABLE III

COMPARISON OF PUBLISHED STUDIES WITH THE PROPOSED AACFD METHOD. WHERE PRIOR WORK REPORTS BEAT-TO-BEAT OR INSTANTANEOUS ERRORS RATHER THAN WINDOW-AVERAGED MEAN HR.

Study	Dataset	Sensor/Algorithm	Original Subs./Rec. (Analysis performed on Subs./Rec.)	Error metric(s)	Key remark
This work	AFib (closed)	SCG(z-axis), AACFD	**300 / 300 (300/300)**	MAE [bpm] (10/20/30/60 s): 9.76 / 8.32 / 7.83 / 7.33; RMSE [bpm]: 9.98 / 8.53 / 8.01 / 7.46; R^2 (within/outside AAMI band): $>$ 0.90 / 0.27–0.62	No ECG trace; one telemetry HR value per recording. AF subjects show strong beat-to-beat variability, and many windows fall outside the AAMI $\pm 10\,\%$ HR band.
Kaisti *et al.* [45]	MCG (healthy)	6-DOF MCG: accelerometer + gyroscope fusion	29/29 (29/29)	IBI-level RMSE $\approx$0.10 bpm; MAE not separately reported	99.9 % TP and 99.6 % precision; heavy pre-filtering and dynamic axis selection on multidimensional mechanocardiograms.
Elnaggar *et al.* [25]	MCG (healthy)	SCG(z-axis), CWT+AMPD	29/29 (29/29)	AO-timing RMSE = 57.3 ms; HR MAE = 2.05 bpm (2-s HR windows)	Cross-dataset AO peak detector evaluated per dataset; good performance on healthy MCG.
This work	MCG (healthy)	SCG(z-axis), AACFD	**29/29 (29/29)**	MAE [bpm] (10/20/30/60 s): 1.76 / 0.99 / 0.99 / 0.91; RMSE [bpm]: 2.14 / 1.26 / 1.25 / 1.11; $R^2 \approx 0.99$ (all windows)	Single-axis SCG. One subject shows MAE $\approx$7–9 bpm on 10-s windows due to motion; for most subjects 30-s MAE is < 4.5 bpm.
Parlato *et al.* [16]	MCG+CEBS (healthy)	SCG, fully automated ECG-free template matching	49/49 (49/49)	Sensitivity/PPV (SCG, %): 97.8 / 96.7; IBI slope/intercept: $\approx$1.00 / -1.5 ms; $R^2 = 0.9996$; Bland–Altman bias 0 ms; LoA $\approx [-5.0, 5.4]$ ms	Aggregated healthy SCG from 29 MCG and 20 CEBS subjects; near-perfect beat-to-beat agreement with ECG.
Centracchio *et al.* [38]	VHD (pathological)	3-axis SCG, cross-correlation template matching	100/100 (77/77)	Beat-to-beat timing error ± 7.8 ms ($\sim$0.75 bpm at 60 bpm); HR MAE not reported	23 traces rejected after manual quality screening; IBI-level evaluation without concurrent ECG.
Elnaggar *et al.* [25]	VHD (pathological)	SCG(z-axis), CWT+AMPD	100/100 (99/99)	AO-timing RMSE = 121.7 ms; HR MAE = 8.78 bpm (2-s HR windows)	One outlier subject excluded.
Parlato *et al.* [16]	VHD (pathological)	SCG, fully automated ECG-free template matching	100/100 (77/77)	Sensitivity/PPV 85.2 / 95.1 %; IBI slope 0.997, intercept 3 ms, $R^2 \approx 0.999$; Bland–Altman bias 0 ms; LoA $\approx \pm 11$ ms	Same VHD cohort; 77 SCG recordings retained after automated quality checks.
This work	VHD (pathological)	SCG(z-axis), AACFD	**100/100 (100/100)**	MAE [bpm] (10/20/30/60 s): 5.28 / 4.33 / 4.38 / 3.97; RMSE [bpm]: 6.00 / 4.82 / 4.75 / 4.24; R^2 (within/outside AAMI band): 0.97–0.98 / 0.43–0.55	All recordings retained; $\sim$14–18 % of subjects lie outside the AAMI $\pm 10\,\%$ band due to very noisy or arrhythmic traces.
This work†	VHD (Centracchio subset)	SCG(z-axis), AACFD	**100/100 (77/77)**	MAE [bpm] (10/20/30/60 s): 3.32 / 2.64 / 2.56 / 2.26; RMSE [bpm]: 3.96 / 3.05 / 2.90 / 2.52	Same 77 recordings as retained in [38].
This work‡	VHD (quality-screened; 77-recording subset)	SCG(z-axis), AACFD	**100/100 (77/77)**	MAE [bpm] (10/20/30/60 s): 1.81 / 1.22 / 1.13 / 0.99; RMSE [bpm]: 2.27 / 1.53 / 1.41 / 1.20; $R^2 \approx 0.99$ (retained subset)	Our screening discards 23 low-quality recordings, yielding a 77-recording subset that is overlapping but not identical to the one in [38]; on this subset AACFD reaches $\sim$1 bpm MAE on 20–60-s windows.
This work	MC-SCG (healthy)	$\mathrm{SCG}_{(2\text{–}3\text{–}Z)}$, AACFD	**13/13 (13/13)**	MAE [bpm] (10/20/30/60 s): 11.99 / 15.22 / 14.43 / 14.68; RMSE [bpm]: 13.53 / 16.07 / 15.07 / 14.95; R^2 (in 9 / out 4): 0.98–0.99 / 0.06–0.99	First SCG-only HR results on this imaging dataset; strong motion and ECG issues in several subjects lead to large errors.
Elnaggar *et al.* [25]	MC-SCG (screened)	$\mathrm{SCG}_{(2\text{–}3\text{–}Z)}$, CWT+AMPD	13/13 (9/9)	AO-timing RMSE = 37.2 ms; HR MAE = 1.43 bpm (2-s HR windows)	Nine recordings retained after automatic quality checks.
This work†	MC-SCG (screened)	$\mathrm{SCG}_{(2\text{–}3\text{–}Z)}$, AACFD	**13/13 (9/9)**	MAE [bpm] (10/20/30/60 s): 1.86 / 1.16 / 1.34 / 0.98; RMSE [bpm]: 2.38 / 1.53 / 1.69 / 1.16; $R^2 \approx 0.99$ (retained 9 recordings)	Same 9 recordings as retained in [25]. AACFD achieves sub-bpm MAE on 20–60-s windows.
Sandelin *et al.* [47]	CEBS (healthy)	CNN on real + synthetic MCG/SCG	20/60 (20/60)	MAE $\approx$1.12 bpm (windowed HR; exact window length differs); RMSE not reported	Hybrid synthetic–real training; focuses on peak detection rather than explicit SCG-only window HR benchmarking.
Pustozerov *et al.* [39]	CEBS (healthy)	Adaptive preprocessing + ECG-derived peak ranking	20/60 (20/60)	Rest: HR difference 0.9 $\pm$ 2.4 bpm; reading-aloud task: 6.45 $\pm$ 3.01 bpm; MAE/RMSE not separated	SCG processed using algorithms originally designed for ECG; performance degrades markedly under light activity.
Elnaggar *et al.* [25]	CEBS (healthy)	SCG(z-axis), CWT+AMPD	20/60 (20/60)	AO-timing RMSE = 33.9 / 33.1 / 41.7 ms; HR MAE = 1.48 / 1.41 / 1.74 bpm (2-s windows; basal/post/music)	Phase-wise analysis; consistently low HR MAE across protocol segments with 2-s HR windows.
This work	CEBS (healthy)	SCG(z-axis), AACFD	**20/60 (20/60)**	MAE [bpm] (10/20/30/60 s): 1.26 / 0.88 / 0.72 / 0.57; RMSE [bpm]: 1.58 / 1.10 / 0.89 / 0.68; $R^2 \approx 0.99$ (all windows)	All recordings within AAMI $\pm 10\,\%$ band; highest per-subject MAE 2.46 bpm (b018/p018) on 30-s windows.
Elnaggar *et al.* [25]	RHC (pathological)	SCG(z-axis), CWT+AMPD	73/82 (72/81)	AO-timing RMSE = 183.1 ms; HR MAE = 11.06 bpm (2-s HR windows)	One subject and one recording excluded after preprocessing.
This work	RHC (pathological)	SCG(z-axis), AACFD	**73/82 (73/82)**	MAE [bpm] (10/20/30/60 s): 4.68 / 3.74 / 3.58 / 3.30; RMSE [bpm]: 6.02 / 4.78 / 4.55 / 4.00; R^2 (within/outside AAMI band): $\approx$ 0.98 / 0.02–0.12	First SCG-based mean-HR benchmark on this cohort using non-overlapping 10–60-s windows; 68/70/72/71 of 82 recordings lie within the AAMI $\pm 10\,\%$ band for 10/20/30/60-s windows.
This work†	RHC (screened subset)	SCG(z-axis), AACFD	**73/82 (69/77)**	MAE [bpm] (10/20/30/60 s): 3.57 / 2.63 / 2.46 / 2.21; RMSE [bpm]: 4.70 / 3.46 / 3.20 / 2.73; $R^2 \approx 0.98$ on retained recordings	After removing traces with clear SCG/ECG problems (TRM223-RHC1, TRM235-RHC1, TRM245-RHC1, TRM246-RHC1, TRM166-RHC1), MAE approaches 2–3 bpm on 20–60-s windows.

Notes: Rows marked † or ‡ report performance after excluding clearly corrupted or extreme-error recordings based on ECG/SCG quality checks. For VHD, [38] excluded 23 recordings; our exclusion list also removes 23 but differs on 13 recordings. Relative to [38] we *retain* CP-06, CP-17, CP-18, CP-25, CP-35, CP-46, CP-50, CP-51, CP-54, UP-02, UP-03, UP-26, UP-28, and instead *exclude* CP-14, CP-16, CP-22, CP-23, CP-33, CP-43, CP-48, CP-52, CP-55, CP-56, UP-01, UP-10, UP-17. All "This work" errors are per-subject mean MAE/RMSE computed from non-overlapping SCG windows of the stated duration (10, 20, 30, and 60 s).

arising from motion bursts or transient ECG/SCG mismatches.

Finally, AACFD is deliberately tuned to retain as many clinically usable windows as possible. Combined ECG- and SCG-based quality control discards only windows with clearly unusable signal morphology; as a result, more than 90% of all non-overlapping 10–60 s windows are kept across all datasets (Table II). The reported errors therefore reflect performance on the majority of the recording duration, including moderately noisy windows, rather than on a few hand-picked clean segments.

V. Results

Table II reports window coverage for each dataset; the notation "CEBS(20/60)" denotes 20 subjects and 60 recordings, and similarly for the other datasets.

As summarized in Table II, the combined ECG- and SCG-based quality control removes only a small fraction of windows in all six datasets. For every window duration between 10 and 60 s, more than 90% of non-overlapping windows are retained, with typical coverage around 93–95%. Even in the arrhythmic AFib smartphone cohort and the motion-rich MC-SCG and RHC datasets, AACFD delivers a valid HR estimate in almost every window, and all 60-s AFib windows are accepted. This high window coverage ensures that the MAE and RMSE values reported in this section are computed from nearly the entire usable recording time rather than from a small number of particularly clean segments. This coverage pattern also reflects a deliberate design choice in how AACFD is evaluated. Many SCG-based beat-detection or template-matching pipelines first identify short, high-quality segments and either ignore or down-weight windows that do not meet strict regularity criteria. In contrast, our benchmark applies AACFD to essentially all non-overlapping 10–60 s windows and discards only those with clearly unusable ECG or SCG. As a result, the reported window-level HR errors reflect performance under realistic conditions, including moderate motion and morphology variability, rather than being restricted to a small subset of idealized windows.

Unless otherwise stated, all MAE and RMSE values reported below refer to differences between SCG-derived and ECG-derived *mean* HR values in non-overlapping windows of the stated duration (10, 20, 30, or 60 s), not to instantaneous beat-to-beat errors. Two sets of error metrics are reported: (i) all-recordings results, and (ii) quality-screened results obtained after discarding traces that failed objective criteria. A recording was excluded when it reliably indicated heavy motion artifacts, sensor saturation, or mis-annotated/low-SNR ECG.

Per-subject MAE distributions for the six datasets are shown as violin plots in Fig. 2a–Fig. 2f, and Bland–Altman plots in Fig. 3a–Fig. 3f. Dataset-averaged MAE before and after outlier handling is summarized in Fig. 4.

The AFib dataset has an overall MAE of 9.76 / 8.32 / 7.83 / 7.33 bpm averaged across 300 subjects for 10, 20, 30, and 60 s windows respectively. Fig. 2a shows the full per-subject distribution, while Fig. 3a shows that 74 out of 150 AF subjects and 126 out of 150 SR subjects are within the tolerance of $\pm 10\%$ of the reference HR, as per the AAMI (Association for the Advancement of Medical Instrumentation) guidelines [49]. For subjects within the tolerance band, the squared Pearson correlation (R^2) between SCG and reference HR is above 0.90; for out-of-tolerance subjects it ranges from 0.27 to 0.62. The MCG dataset has an overall MAE of 1.76, 0.99, 0.99, 0.91 bpm across 29 subjects for 10, 20, 30, and 60 s windows respectively. Fig. 2b shows the violin plot for the MCG dataset. The Bland-Altman plot in Fig. 3b shows that only 2 out of 29 subjects have an MAE of $> \pm 10\%$ bpm for 10 s only and all subjects are within the band for 20–60 s. Moreover, the R^2 is almost 0.99 for all subjects in all windows. The VHD dataset has an MAE of 5.28, 4.33, 4.38, and 3.97 bpm for 10, 20, 30, and 60 s windows, respectively, across all 100 subjects. Fig. 2c shows a broader distribution than for the MCG or CEBS dataset, and Fig. 3c shows that CP-24, CP-29, and few other subjects out of 100 subjects are out of the $\pm 10\%$ bpm MAE range through Bland-Altman plot for 10, 20, 30, and 60 s respectively. For subjects within the tolerance band, R^2 is 0.97–0.98, while for out-of-band subjects it typically lies between 0.43 and 0.55. The MC-SCG dataset has an MAE of 11.99, 15.22, 14.43, 14.68 bpm, as shown in Fig. 2d for 10, 20, 30, and 60 s windows respectively, whereas Fig. 3d shows that 9 out of 13 subjects are within the AAMI band, with R^2 between 0.98 and 0.99; the remaining subjects have strongly corrupted ECG/SCG, and their R^2 values range from 0.06 to 0.99 depending on window length. For CEBS dataset, the overall MAE across 20 subjects and 60 recordings is 1.26, 0.88, 0.72, 0.57 bpm for 10, 20, 30, and 60 s windows; no subject lies outside the $\pm 10\,\%$ range for any window length (Fig. 3e), and R^2 is close to 0.99 for all windows. The RHC dataset, which has 73 subjects (82 recordings) in total, yields an MAE of 4.68, 3.74, 3.58, and 3.30 bpm (Fig. 2f). As shown in Fig. 3f, 68, 70, 72, and 71 recordings out of 82 fall within the AAMI $\pm 10\,\%$ band for 10, 20, 30, and 60 s windows, respectively. For windows within the band, the global R^2 is approximately 0.98, whereas for out-of-band windows R^2 is much lower (0.02–0.12). Across all datasets, the lowest 10 s R^2 values are observed in RHC, reflecting the strong motion and hemodynamic variability in this cohort.

The per-dataset impact of trace screening is summarised in Fig. 4. In AFib, the highest per-subject MAE is 66.8 bpm (AF subject). In MCG, subjects 9 and 19 reach MAE values of 7–9 bpm for 10 s windows, likely due to motion artifacts; all other subjects remain below 4.5 bpm. In VHD, the largest average MAE values occur in CP-24 (77 bpm), CP-29 (35 bpm), and CP-31 (30 bpm). Applying our own ECG/SCG-based screening and removing 23 clearly corrupted recordings reduces the overall MAE to 1.81, 1.22, 1.13, and 0.99 bpm, and the RMSE to 2.27, 1.53, 1.41, and 1.20 bpm for 10, 20, 30, and 60 s windows, respectively. If instead we remove the 23 traces excluded in [38], i.e., use their 77-subject subset, AACFD yields MAE values of 3.32, 2.64, 2.56, and 2.26 bpm and RMSE values of 3.96, 3.05, 2.90, and 2.52 bpm for 10, 20, 30, and 60 s windows, respectively. In MC-SCG, subjects 7–10 contain clearly corrupted ECG; excluding them reduces the MAE to 1.86, 1.16, 1.34, and 0.98 bpm for 10, 20, 30, and 60 s windows. In CEBS, subjects b018 and p018 exhibit the highest per-subject MAE (2.46 bpm). For RHC, the MAE on

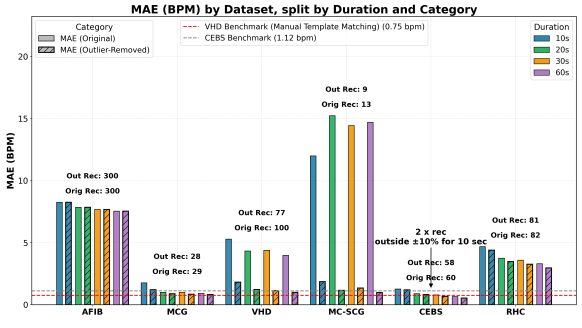

Fig. 4. Dataset-averaged MAE for non-overlapping windows of 10, 20, 30, and 60 s. For each dataset and duration, solid bars show MAE and hatched bars show MAE after ECG and SCG based outlier handling and temporal-consistency refinement.

all 82 recordings is 4.68, 3.74, 3.58, and 3.30 bpm for 10, 20, 30, and 60 s windows. After removal of TRM223-RHC1 the MAE reduced to 4.39, 3.47, 3.26, 2.96 bpm for 10, 20, 30, and 60 s windows respectively. Further excluding TRM235-RHC1, TRM245-RHC1, TRM246-RHC1, and TRM166-RHC1 (77 recordings in total) reduces the MAE to 3.57, 2.63, 2.46, and 2.21 bpm.

VI. Discussion

The window-based evaluation highlights both the strengths and limitations of AACFD. On controlled datasets with good signal quality (MCG and CEBS), the hybrid YIN and ACF pipeline achieves sub-bpm MAE on 20–60 s windows after quality control. On more challenging pathological cohorts (VHD, MC-SCG, RHC), raw errors can be large when heavy motion or poor annotation is present, but refined MAE values around 1–3 bpm indicate that the underlying SCG contains sufficient information for reliable mean HR estimation once obviously corrupted windows are rejected. Autocorrelation itself is of course a classical tool, and it was used both as a feature source in our earlier smartphone mechanocardiography classification study [22] and as the core component of a preliminary single-recording HR estimator on smartphone accelerometer data [24]. Neither of these works, however, implemented the hybrid YIN and ACF design, morphology-based harmonic guard, or cross-dataset window-level benchmarking reported here, nor did they provide systematic window-based SCG–ECG HR error analyses. The AACFD pipeline presented in this paper therefore represents a distinct and more general development building on those preliminary ideas.

A. Comparison With Prior Work

On the MCG dataset, Kaisti *et al.* fused accelerometer and gyroscope channels and combined envelope- and morphology-based detectors, achieving an inter-beat-interval RMSE of 5.6 ms (HR RMSE $\approx$0.1 bpm) in healthy subjects [45]. Our single-axis SCG implementation, without gyroscope fusion, attains refined MAE below 1 bpm on 20–60 s windows, which is weaker than multi-axis peak-detection performance but still competitive for normal HR monitoring.

On CEBS, Sandelin *et al.* reported MAE $\approx$1.1 bpm using CNNs trained on real and synthetic mechanocardiograms [47], while Pustozerov *et al.* found that ECG-derived peak detectors adapted to SCG yielded 0.9 $\pm$ 2.4 bpm at rest but degraded to 6.45 $\pm$ 3.01 bpm during a reading-aloud task [39]. AACFD achieves refined MAE of 0.72 bpm on 30 s CEBS windows using a purely analytical pipeline and a single SCG axis, confirming that carefully designed signal processing can match or exceed more complex methods in controlled conditions.

For the VHD dataset, Centracchio *et al.* used ECG-free template matching on 3-axis SCG and obtained millisecond-level timing errors on 77 of 100 subjects, but required manual template selection and rejected low-quality traces [38]. When AACFD is evaluated on the same 77-subject subset, the 10/20/30/60 s MAE becomes 3.32/2.64/2.56/2.26 bpm and the corresponding RMSE is 3.96/3.05/2.90/2.52 bpm. Using our own ECG/SCG-based quality checks to define a different 77-subject subset yields lower MAE of 1.81/1.22/1.13/0.99 bpm and RMSE of 2.27/1.53/1.41/1.20 bpm. Both analyses are consistent with the observation in [38] that a sizeable fraction of VHD recordings is extremely noisy, and that once those traces are removed, mean-HR errors can approach $\sim$1 bpm on 20–60 s windows.

The invasive RHC cohort remains challenging: even after refinement, 30 s windows yield a mean MAE of 2.46 bpm. This is unsurprising given procedure-related motion, changes in hemodynamics, and potential mismatches between the wearable SCG and invasive reference timing. Nevertheless, errors are still within the AAMI tolerance (the lesser of ± 10 % or ± 5 bpm) for a large fraction of recordings.

Beyond the works included in Table III, several recent studies have reported beat-to-beat HR and HRV estimation from SCG on other datasets. Choudhary *et al.* derived HRV indices from SCG and showed the feasibility of HRV analysis from chest vibrations [9]. Lin and Jhou jointly estimated heart and respiratory rates from resting SCG [10], while Sieciński *et al.* compared HRV indices from SCG and ECG on the CEBS database [11]. Wahlström *et al.* used a hidden Markov model for SCG beat detection [12], Cocconcelli *et al.* proposed a high-accuracy unsupervised annotation strategy [13], and Schipper *et al.* and Zheng *et al.* introduced advanced probabilistic and AO-based detectors for cardiomechanical signals [14], [15]. Parlato *et al.* recently presented a fully automated template-matching framework for ECG-free heartbeat detection in healthy and pathological cardiomechanical signals [16]. All these methods operate at the beat level and primarily target instantaneous HR or HRV; their error metrics are therefore not directly comparable with the window-averaged MAE/RMSE reported here, but they demonstrate that SCG can support high-resolution timing under controlled conditions. AACFD is complementary, focusing on robust mean HR across heterogeneous cohorts and sensor setups using a single SCG axis.

B. Mean HR Versus Instantaneous HR

A key limitation of the present work is that AACFD is evaluated on *window-averaged* HR, not instantaneous beat-to-beat HR. Although the internal YIN and ACF branches operate on 3-s segments and could support higher temporal

resolution, all reported metrics are based on 10–60 s windows and therefore cannot be used directly to derive standard HRV indices. This must be stated explicitly: our goal is robust estimation of mean HR at clinically relevant time scales for wearable and home monitoring, not detailed HRV analysis. Extending AACFD to provide reliable beat-to-beat intervals from SCG, especially during arrhythmia and motion, is an important direction for future work.

C. Sources of Error and Practical Implications

Large errors in some AFib, VHD, MC-SCG, and RHC recordings arise from three main sources: (i) severe motion artifacts or poor sensor contact that corrupt SCG morphology, (ii) mismatches between SCG and ECG or clinical HR annotations, and (iii) intrinsic beat-to-beat variability in arrhythmias such as AF, which makes a single reference HR per window less representative. Our ECG- and SCG-based quality indices, together with temporal-consistency refinement, substantially reduce these errors but cannot fully correct recordings with fundamentally unreliable reference or signal content.

Clinically, AACFD is not intended to replace 3–12-lead ECG, which remains the gold standard for rhythm analysis and diagnostic decision-making. Its purpose is to provide a low-cost, SCG-based fallback or complement in settings where ECG or PPG are unreliable or impractical: opportunistic checks with a smartphone on the sternum, redundancy in chest-worn wearables, or long-term home monitoring where only a single inertial axis is available. Embedding AACFD into existing systems requires only one chest accelerometer channel and modest on-device processing; all steps in Algorithm 1 are simple time-domain and envelope operations with modest memory requirements, making real-time implementation on contemporary microcontrollers and wearable platforms feasible. The per-window computational cost is linear in the number of samples, so AACFD can run continuously on typical wearable-class Microcontroller Units without dedicated accelerators. The AFib and RHC cohorts in particular show that AACFD in its current form is not a complete solution for strongly arrhythmic or highly dynamic recordings: mean-HR errors remain in the 5–10 bpm range for some subjects even after quality screening. Handling such challenging regimes will require either explicit arrhythmia modelling, which we view as future work beyond the present mean-HR focus.

D. Limitations and Future Work

Other limitations include evaluation on mostly supine or semi-supine recordings, reliance on down-sampling all SCG signals to 200 Hz, and the use of hand-tuned thresholds in some robustness checks. Future work will address these limitations by (i) validating AACFD in fully ambulatory recordings with stronger motion, (ii) extending the framework to multi-axis accelerometer–gyroscope fusion, and (iii) exploring data-driven refinements (e.g., learned fusion weights or SQI mapping) while keeping the core pipeline interpretable.

VII. Conclusion

This study provides a multi-dataset evaluation of SCG-based heart-rate estimation in conditions ranging from healthy supine subjects to patients with valvular disease, arrhythmias, and invasive right-heart catheterization. The proposed AACFD method combines a YIN-style envelope analysis with a short-window autocorrelation branch, guided by signal-quality indices and simple morphology-based harmonic guards, to estimate mean HR from a single SCG axis without ECG calibration or machine learning.

Throughout this work we deliberately restrict the scope to *window-averaged* HR on 10–60 s windows; AACFD is not intended to provide beat-to-beat timing or heart-rate-variability indices in its current form.

On controlled datasets, AACFD achieves sub-bpm MAE on 20–60 s windows, and on several pathological cohorts it maintains clinically acceptable accuracy once heavily corrupted windows are removed based on ECG and SCG quality criteria. At the same time, the method remains lightweight enough for real-time implementation on commodity hardware and embedded devices.

Future work will therefore focus on extending AACFD towards reliable beat-to-beat timing, multi-axis accelerometer–gyroscope fusion, and validation in fully ambulatory conditions where motion artifacts and posture changes are dominant. A longer-term goal is to integrate SCG-based mean-HR monitoring into multi-modal wearable platforms alongside ECG and PPG, providing redundant, interpretable HR estimates that remain robust when any single modality is compromised.

References

[1] G. Grouios, E. Ziagkas, A. Loukovitis, K. Chatzinikolaou, and E. Koidou, "Accelerometers in our pocket: Does smartphone accelerometer technology provide accurate data?," *Sensors*, vol. 23, no. 1, Art. no. 0192, Jan. 2022, doi: 10.3390/s23010192.

[2] O. T. Inan *et al.*, "Ballistocardiography and seismocardiography: A review of recent advances," *IEEE J. Biomed. Health Inform.*, vol. 19, no. 4, pp. 1414–1427, Jul. 2015, doi: 10.1109/JBHI.2014.2361732.

[3] J. M. Zanetti and K. Tavakolian, "Seismocardiography: Past, present and future," in *Proc. Annu. Int. Conf. IEEE Eng. Med. Biol. Soc.*, Osaka, Japan, Jul. 2013, pp. 7004–7007, doi: 10.1109/EMBC.2013.6611170.

[4] C. Yang and N. Tavassolian, "Combined seismo- and gyro-cardiography: A more comprehensive evaluation of heart-induced chest vibrations," *IEEE J. Biomed. Health Inform.*, vol. 22, no. 5, pp. 1466–1475, Sep. 2018, doi: 10.1109/JBHI.2017.2764798.

[5] G. Prieto-Avalos *et al.*, "Wearable devices for physical monitoring of heart: A review," *Biosensors*, vol. 12, no. 5, Art. no. 292, May 2022, doi: 10.3390/bios12050292.

[6] A. Taebi, B. E. Solar, A. J. Bomar, R. H. Sandler, and H. A. Mansy, "Recent advances in seismocardiography," *Vibration*, vol. 2, no. 1, pp. 64–86, Jan. 2019, doi: 10.3390/vibration2010005.

[7] R. M. Rangayyan and S. Krishnan, "Introduction to biomedical signals," in *Biomedical Signal Analysis*. Hoboken, NJ, USA: Wiley, 2024, pp. 1–69, doi: 10.1002/9781119825883.ch1.

[8] P. H. Charlton, T. P. Velardo, G. Abbas *et al.*, "The 2023 wearable photoplethysmography roadmap," *Physiol. Meas.*, vol. 44, no. 11, Art. no. 111001, 2023, doi: 10.1088/1361-6579/acead2.

[9] T. Choudhary, M. Das, L. N. Sharma, and M. K. Bhuyan, "Analyzing seismocardiographic approach for heart rate variability measurement," *Biomed. Signal Process. Control*, vol. 68, Art. no. 102793, 2021, doi: 10.1016/j.bspc.2021.102793.

[10] Y.-D. Lin and Y.-F. Jhou, "Estimation of heart rate and respiratory rate from the seismocardiogram under resting state," *Biomed. Signal Process. Control*, vol. 57, Art. no. 101779, 2020, doi: 10.1016/j.bspc.2019.101779.

[11] S. Sieciński, E. J. Tkacz, and P. S. Kostka, "Comparison of HRV indices obtained from ECG and SCG signals from CEBS database," *BioMed Eng. OnLine*, vol. 18, Art. no. 69, 2019, doi: 10.1186/s12938-019-0687-5.

[12] J. Wahlström, I. Skog, P. Händel, and T. Bengtsson, "A hidden Markov model for seismocardiography," *IEEE Trans. Biomed. Eng.*, vol. 64, no. 10, pp. 2361–2372, Oct. 2017, doi: 10.1109/TBME.2017.2648741.

[13] F. Cocconcelli, N. Mora, G. Matrella, and P. Ciampolini, "High-accuracy, unsupervised annotation of seismocardiogram traces for heart rate monitoring," *IEEE Trans. Instrum. Meas.*, vol. 69, no. 5, pp. 6372–6380, May 2020, doi: 10.1109/TIM.2020.2967135.

[14] F. Schipper, R. J. G. van Sloun, A. Grassi *et al.*, "Maximum a posteriori detection of heartbeats from a chest-worn accelerometer," *Physiol. Meas.*, vol. 45, Art. no. 035009, 2024, doi: 10.1088/1361-6579/ad2f5e.

[15] C. Zheng, Y. Li, Z. Du *et al.*, "High accurate detection method for aortic valve opening of seismocardiography signals," *Biomed. Signal Process. Control*, vol. 87, Art. no. 105484, 2024, doi: 10.1016/j.bspc.2023.105484.

[16] S. Parlato, P. Bifulco, G. Cesarelli *et al.*, "Fully automated template matching method for ECG-free heartbeat detection in cardiomechanical signals of healthy and pathological subjects," *Phys. Eng. Sci. Med.*, vol. 48, pp. 649–664, 2025, doi: 10.1007/s13246-025-01531-3.

[17] IEEE DataPort, "Mechanocardiograms with ECG reference," [Online]. Available: https://ieee-dataport.org/documents/mechanocardiograms-ecg-reference.

[18] PhysioNet, "Combined measurement of ECG, breathing and seismocardiograms v1.0.0," [Online]. Available: https://physionet.org/content/cebsdb/1.0.0/ (accessed Mar. 24, 2025).

[19] PhysioNet, "SCG-RHC: Wearable seismocardiogram signal and right-heart catheter database v1.0.0," [Online]. Available: https://physionet.org/content/scg-rhc-wearable-database/1.0.0/ (accessed Mar. 24, 2025).

[20] C. Yang *et al.*, "An open-access database for the evaluation of cardio-mechanical signals from patients with valvular heart diseases," *Front. Physiol.*, vol. 12, Art. no. 750221, Sep. 2021, doi: 10.3389/fphys.2021.750221.

[21] K. Munck, K. Sørensen, J. J. Struijk, and S. E. Schmidt, "Data for: Multichannel seismocardiography: An imaging modality for investigating heart vibrations," *Mendeley Data*, V1, 2020, doi: 10.17632/SCN464X7XD.1.

[22] Z. Iftikhar, O. Lahdenoja, M. J. Tadi *et al.*, "Multiclass classifier based cardiovascular condition detection using smartphone mechanocardiography," *Sci. Rep.*, vol. 8, Art. no. 9344, 2018, doi: 10.1038/s41598-018-27683-9.

[23] J. Jaakkola *et al.*, "Mobile phone detection of atrial fibrillation with mechanocardiography: The MODE-AF study," *Circulation*, vol. 137, no. 14, pp. 1524–1527, Apr. 2018, doi: 10.1161/CIRCULATIONAHA.117.032804.

[24] A. Ullah *et al.*, "Heart rate estimation through autocorrelation from single axis accelerometer of smartphone," in *Proc. 47th Annu. Int. Conf. IEEE Eng. Med. Biol. Soc. (EMBC)*, Copenhagen, Denmark, 2025, pp. 1–4, doi: 10.1109/EMBC58623.2025.11253255.

[25] I. Elnaggar, S. Seifizarei, J. Sandelin *et al.*, "Cross-dataset validation of a sensor-agnostic seismocardiography peak detection method," in *Proc. IEEE/ACM Conf. Connected Health: Applications, Systems and Engineering Technologies (CHASE)*, New York, NY, USA, Jun. 2025, pp. 395–400, doi: 10.1145/3721201.3724416.

[26] D. Salerno and J. Zanetti, "Seismocardiography: A new technique for recording cardiac vibrations—concept, method, and initial observations," *Clin. Cardiol.*, vol. 13, pp. 623–625, Aug. 1990.

[27] D. M. Salerno and J. Zanetti, "Seismocardiography for monitoring changes in left-ventricular function during ischemia," *Chest*, vol. 100, no. 4, pp. 991–993, Oct. 1991, doi: 10.1378/chest.100.4.991.

[28] I. Starr, A. J. Rawson, H. A. Schroeder, and N. R. Joseph, "Studies on the estimation of cardiac output in man, and of abnormalities in cardiac function, from the heart's recoil and the blood's impacts; the ballistocardiogram," *Am. J. Physiol.*, vol. 127, no. 1, pp. 1–28, Jul. 1939, doi: 10.1152/ajplegacy.1939.127.1.1.

[29] K. Sørensen and K. Munck, *Seismocardiography: Interpretation and Clinical Application*. Aalborg, Denmark: Aalborg Univ., 2021, Tech. Rep., doi: 10.54337/AAU451017905.

[30] M. Á. García-González, A. Argelagós-Palou, M. Fernández-Chimeno, and J. J. Ramos-Castro, "A comparison of heartbeat detectors for the seismocardiogram," in *Comput. Cardiol.*, Zaragoza, Spain, Sep. 2013, vol. 40, pp. 461–464.

[31] J. G. Proakis and D. G. Manolakis, *Digital Signal Processing: Principles, Algorithms, and Applications*, 4th ed. Boston, MA, USA: Pearson, 2014.

[32] A. Ullah *et al.*, "ExoMechHand prototype development and testing with EMG signals for hand rehabilitation," *Med. Eng. Phys.*, vol. 124, Art. no. 104095, Feb. 2024, doi: 10.1016/j.medengphy.2023.104095.

[33] D. Rai *et al.*, "A comprehensive review on seismocardiogram: Current advancements on acquisition, annotation, and applications," *Mathematics*, vol. 9, no. 18, Art. no. 2243, Sep. 2021, doi: 10.3390/math9182243.

[34] M. Laurino *et al.*, "Moving auto-correlation window approach for heart-rate estimation in ballistocardiography extracted by mattress-integrated accelerometers," *Sensors*, vol. 20, no. 18, Art. no. 5438, Sep. 2020, doi: 10.3390/s20185438.

[35] S. Seifizarei *et al.*, "Continuous radar-based heart-rate monitoring using an autocorrelation algorithm in the intensive care unit," *IEEE J. Biomed. Health Inform.*, Early Access, 2025, doi: 10.1109/JBHI.2025.3527566.

[36] Y. D'Mello *et al.*, "Autocorrelated differential algorithm for real-time seismocardiography analysis," *IEEE Sens. J.*, vol. 19, no. 13, pp. 5127–5140, Jul. 2019, doi: 10.1109/JSEN.2019.2903449.

[37] X. Wen, Y. Huang, X. Wu, and B. Zhang, "A correlation-based algorithm for beat-to-beat heart-rate estimation from ballistocardiograms," in *Proc. IEEE Eng. Med. Biol. Conf.*, Berlin, Germany, Jul. 2019, pp. 6355–6358, doi: 10.1109/EMBC.2019.8856464.

[38] J. Centracchio *et al.*, "ECG-free heartbeat detection in seismocardiography signals via template matching," *Sensors*, vol. 23, no. 10, Art. no. 4684, May 2023, doi: 10.3390/s23104684.

[39] E. Pustozerov, U. Kulau, and U. V. Albrecht, "Automated heart-rate detection in seismocardiograms using electrocardiogram-based algorithms—A feasibility study," *Bioengineering*, vol. 11, no. 6, Art. no. 596, Jun. 2024, doi: 10.3390/bioengineering11060596.

[40] R. K. Pearson, Y. Neuvo, J. Astola, and M. Gabbouj, "Generalized Hampel filters," *EURASIP J. Adv. Signal Process.*, vol. 2016, Art. no. 87, 2016, doi: 10.1186/s13634-016-0383-6.

[41] F. R. Hampel, "The influence curve and its role in robust estimation," *J. Amer. Stat. Assoc.*, vol. 69, no. 346, pp. 383–393, Jun. 1974.

[42] V. Chandola, A. Banerjee, and V. Kumar, "Anomaly detection: A survey," *ACM Comput. Surv.*, vol. 41, no. 3, Art. no. 15, pp. 1–58, Jul. 2009, doi: 10.1145/1541880.1541882.

[43] H. Qarib and H. Adeli, "A comparative study of signal-processing methods for structural-health monitoring," *J. Vibroengineering*, vol. 18, no. 4, pp. 2186–2204, Jun. 2016, doi: 10.21595/jve.2016.17218.

[44] L. Lu *et al.*, "Uncertainties in the analysis of heart-rate variability: A systematic review," *IEEE Rev. Biomed. Eng.*, vol. 17, pp. 180–196, 2024, doi: 10.1109/RBME.2023.3271595.

[45] M. Kaisti *et al.*, "Stand-alone heartbeat detection in multidimensional mechanocardiograms," *IEEE Sens. J.*, vol. 19, no. 1, pp. 234–242, Jan. 2019, doi: 10.1109/JSEN.2018.2874706.

[46] S. Parlato *et al.*, "Heartbeat detection in gyrocardiography signals without concurrent ECG tracings," *Sensors*, vol. 23, no. 13, Art. no. 6200, Jul. 2023, doi: 10.3390/s23136200.

[47] J. Sandelin, I. Elnaggar, O. Lahdenoja, M. Kaisti, and T. Koivisto, "Generating synthetic mechanocardiograms for machine-learning-based peak detection," *IEEE Sens. Lett.*, Early Access, 2024, doi: 10.1109/LSENS.2024.3443526.

[48] D. Makowski, T. Pham, Z. J. Lau, J. C. Brammer, F. Lespinasse, H. Pham, C. Schölzel, and S. H. A. Chen, "NeuroKit2: A Python toolbox for neurophysiological signal processing," *Behav. Res. Methods*, vol. 53, no. 4, pp. 1689–1696, Aug. 2021, doi: 10.3758/s13428-020-01516-y.

[49] "ANSI/AAMI/ISO EC13:2002 (R)2007 – Cardiac Monitors, Heart Rate Meters, and Alarms (Corrected Copy: 25 February 2008)," Accessed: Jan. 22, 2025. [Online]. Available: https://webstore.ansi.org/standards/aami/ansiaamiisoec1320022007